

Determination of the valence band offset at cubic CdSe/ZnTe type II heterojunctions: A combined experimental and theoretical approach

Daniel Mourad,^{1,*} Jan-Peter Richters,² Lionel Gérard,³ Régis André,³ Joël Bleuse,² and Henri Mariette³

¹*Institute for Theoretical Physics, University of Bremen, Otto-Hahn-Allee 1, 28359 Bremen, Germany*

²*CEA-CNRS group 'Nanophysique et Semiconducteurs', CEA-Grenoble, INAC, SP2M, 17 Rue des Martyrs, 38054 Grenoble CEDEX 9, France*

³*CEA-CNRS group 'Nanophysique et Semiconducteurs', Institut Néel-CNRS/Université Joseph Fourier, 25 Rue des Martyrs, 38042 Grenoble CEDEX 9, France*

We present a combined experimental and theoretical approach for the determination of the low-temperature valence band offset (VBO) at CdSe/ZnTe heterojunctions with underlying zincblende crystal structure. On the experimental side, the optical transition of the type II interface allows for a precise measurement of the type II band gap. We show how the excitation-power dependent shift of this photoluminescence (PL) signal can be used for any type II system for a precise determination of the VBO. On the theoretical side, we use a refined empirical tight-binding parametrization in order to accurately reproduce the band structure and density of states around the band gap region of cubic CdSe and ZnTe and then calculate the branch point energy (also known as charge neutrality level) for both materials. Because of the cubic crystal structure and the small lattice mismatch across the interface, the VBO for the material system under consideration can then be obtained from a charge neutrality condition, in good agreement with the PL measurements.

PACS numbers: 78.55.Et, 71.20.Nr, 71.15.Ap, 73.40.Lq

Keywords: valence band offset, type II, heterojunctions, CdSe, ZnTe, photoluminescence, tight-binding

I. INTRODUCTION

The knowledge of valence band offsets (VBOs) is crucial for the design of efficient semiconductor devices, especially when dealing with type II band gap alignment. In general, two possibilities exist for the band alignment of semiconductors. The most widely investigated are the so-called type I systems, in which the narrower gap material plays the role of the potential well for both the electrons and holes, as its conduction band (CB) minimum/valence band (VB) maximum lies at a lower/higher energy than the respective counterparts of the material with the larger gap. There exists, however, another group of semiconductor structures known as type II structures, in which the band gap regions are staggered across the interface normal direction, i. e. the CB minimum and the VB maximum of one material are both at lower energies than the corresponding quantities of the second material (the so-called type III or broken-gap alignments, where the CB minimum of one material dips even below the VB maximum of its counterpart can be considered a special case of type II alignments). Thus for type II alignment, electron and hole wavefunctions are spatially separated across the interface. This separation gives rise to relatively long carrier lifetimes and to a dependence of photoemission and photocurrent on the intensity of excitation, as well as on external electric and magnetic fields. Moreover, type II systems have another important advantage in that they tend to suppress Auger recombination.¹ These properties, as well as other that result from the type II band alignment, provide unique opportunities for new optical properties, e.g. Aharonov-Bohm effects in type II quantum dots,^{2,3} and new potential applications, e.g. for solar cells.^{4,5}

There are many different experimental and theoretical methods to determine the VBO for various material combinations. However, the spread of the calculated values is rather large, as are the results of some experimental methods. The calculation of the VBO at the interface between two semiconductor systems has been an important topic for decades. Although first principle methods⁶ have become more feasible in recent time, they often still lack satisfactory quantitative agreement with experiments, especially for the electronic properties of semiconductors. Furthermore, they do not give insight in the underlying physics at those semiconductor junctions. As a consequence, a lot of effort has been put into models that basically trace the band alignment back to the bulk properties of the constituents by establishing a common reference level. While there exist many works of different levels of sophistication which align the constituents at the junction to vacuum levels,⁷⁻¹⁰ another class of models which calculate the band offset from a charge neutrality condition seems to be more promising nowadays.¹¹⁻¹⁶

The VBO of zincblende CdSe/ZnTe heterojunctions is an important parameter for the simulation of hetero- and nanostructures like colloidal type II nanocrystals.¹⁷ While there are several experimental methods known in order to determine the VBO,¹⁸⁻²⁰ the most widely renowned work on CdSe/ZnTe was performed by Yu et al. who performed X-ray photoelectron spectroscopy (XPS) measurements and found the VBO to be (0.64 ± 0.07) eV at room temperature.²¹ The strongest limitation of XPS measurements is the often poor energy resolution, having an uncertainty of often several 100 meV. Another work by Gleim et al. combines *k*-resolved valence- and core-level photoelectron spectroscopy and gives a simi-

lar result of (0.6 ± 0.1) eV.²² The direct measurement of the optical transition of a type II interface is another method which promises high precision and easy application. Mostly, this method has been used on multi quantum wells made of the In-Al-As-Ga-Sb materials.^{23–25}

In this work, we present a combined theoretical and experimental approach to determine the VBO between CdSe and ZnTe and compare the calculations with the experimentally determined value. The theoretical part presents a refined approach for the calculation of the VBO. It is based on methods known from the literature, but has been improved for a better incorporation of the one-particle properties of the constituents by using a customized empirical tight-binding parametrization. The experimental part utilizes the excitation-dependent measurement of the photoluminescence (PL) signal of the spatially indirect type-II band-gap between CdSe and ZnTe. We introduce a model to correctly extract the type-II band gap from the obtained PL spectra in order to calculate the VBO.

II. EXPERIMENTAL

The samples were fabricated using a Riber 32P molecular beam epitaxy (MBE) machine. First, a 200 nm thick layer of ZnTe is deposited on an InAs substrate under Zn-rich conditions, followed by 400 nm of CdSe under Se-rich conditions. The very low lattice mismatch between cubic CdSe and ZnTe ($a_{\text{CdSe}} = 6.077$ Å and $a_{\text{ZnTe}} = 6.089$ Å, $\Delta a \approx 0.2\%$)²⁶ allows the growth of metastable, cubic CdSe with very good crystal quality,²⁷ as has been confirmed by X-ray diffraction (XRD) and PL measurements.

The PL measurements presented in this work were performed using a frequency doubled Coherent Mira Ti:sapphire fs-laser operating at 810 nm (doubled to 405 nm). The samples are placed in an Oxford liquid Helium cryostat which is mounted on a Zeiss Axiovert 200 inverted microscope. The excitation laser is guided into the microscope using a multi-mode optical fiber. A Zeiss 20x microscope objective focuses the laser on the sample and collects the resulting photoluminescence (PL) signal. The spectral analysis of the PL is performed with a Jobin Yvon Triax 320 spectrometer using an thermoelectrically cooled Andor InGaAs CCD.

III. THEORY

A. Calculation of valence band offsets from the charge neutrality condition

When two semiconductors A and B are brought together to form a common interface, the electronic structure will be altered, as the translational invariance is broken in the direction of the interface normal. Localized interface-induced states with an energy either in the

A or B gap or in the coinciding gap of the constituent semiconductors can be shown to carry net charge density across the junction, thus inducing an interface dipole.²⁸ These states can be interpreted as Bloch-like bulk states of one material that decay exponentially into the other material when crossing the interface.²⁹

Tersoff argued in Ref. 30 that a filled interface state results in local excess charge density, proportional to its conduction character, while an unoccupied state leads to a local charge density deficit proportional to its valence character. At a certain energy, the spectral character of an interface state is of equal CB and VB origin, i. e. neither donor- nor acceptorlike. This energy can thus be identified as the charge neutrality level of the interface states and is commonly called the branch point (BP) energy E_{BP} . Therefore, the orientation of the overall resulting dipole depends on the relative energetic position of the Fermi level to E_{BP} . As the interface states can be traced back to A or B bulk states that reach across the common interface, the BP energy can be seen as an interface-orientation dependent intrinsic property for the given A and B material, respectively.

Similar to other approaches which align materials to the charge neutrality levels of hydrogen impurities (see e. g. Ref. 13), the BP energy can serve as a common reference level for band alignment: The only case where no resulting dipole is left would be the lineup where the BPs of the A and B material coincide (the so-called *canonical lineup*), as all interface dipoles will then cancel out. On the other hand, polarization effects will screen charge transfer effects with a characteristic dielectric constant ϵ , i. e. counteract any deviation from this canonical lineup. As ϵ is relatively high for most compound semiconductors ($\epsilon \approx 10 \dots 20$), the overall charge transfer is effectively reduced and the canonical lineup condition will approximately be fulfilled for most isovalent material combinations, regardless of the stoichiometry-related polarity of the specific interface (see e. g. Ref. 31 for a detailed analysis). If we measure the BP energy $E_{\text{BP}}^{\text{A/B}}$ of each constituent from its VB edge, respectively, the VBO can then be calculated as

$$\Delta E_v \approx E_{\text{BP}}^{\text{B}} - E_{\text{BP}}^{\text{A}} \quad (1)$$

with an accuracy of ~ 0.05 eV.^{30,32} Therefore, the problem of band alignment has approximately been reduced to the separate calculation of E_{BP} for each material.

B. Calculation of branch point energies

According to Allen,³³ the cell-averaged real-space Green's function for the propagation across a surface or interface with normal vector parallel to the direct lattice vector \mathbf{R} is given as

$$G^{\mathbf{R}}(E) = \sum_{n\mathbf{k}} \frac{e^{i\mathbf{k} \cdot \mathbf{R}}}{E - E_n(\mathbf{k})}, \quad (2)$$

where $E_n(\mathbf{k})$ is the band structure, \mathbf{k} the wave vector in the first Brillouin zone (BZ) and n the band index. In accordance with its definition in the preceding subsection, the BP is then given as the energy where the bulk CBs and VBs contribute in equal parts to $G^{\mathbf{R}}(E)$. Although this method allows for the calculation of interface-orientation dependent BP energies, it can be rather tedious numerically, as one has to converge $G^{\mathbf{R}}(E)$ for multiples of the smallest \mathbf{R} for each interface orientation to project out the relevant contributions.³⁴

An alternative is the usage of interface-averaged approximations for the calculation of E_{BP} . Similar to Cardona and Christensen,¹² Schleife et al. generalized previous approaches^{28,35} and calculated the BP as a BZ average of the midgap energy:¹⁴

$$E_{\text{BP}} \approx \frac{1}{2N_{\mathbf{k}}} \sum_{\mathbf{k}} \left[\frac{1}{N_{\text{CB}}} \sum_i^{N_{\text{CB}}} E_{\text{CB}}^i(\mathbf{k}) + \frac{1}{N_{\text{VB}}} \sum_j^{N_{\text{VB}}} E_{\text{VB}}^j(\mathbf{k}) \right]. \quad (3)$$

Here, $N_{\mathbf{k}}$ is number of \mathbf{k} -points and N_{CB} , N_{VB} are the numbers of included CBs and VBs with dispersions $E_{\text{CB}}^i(\mathbf{k})$ and $E_{\text{VB}}^j(\mathbf{k})$, respectively. The \mathbf{k} -sample can be confined to the irreducible wedge of the corresponding BZ, as no interface orientation breaks the symmetry properties of the bulk dispersion, at the expense of losing the orientational dependence. When a sufficiently dense \mathbf{k} -sample is available, Eq. (3) can be reduced to an integration over sufficiently smooth densities of states (DOS),

$$E_{\text{BP}} \approx \frac{1}{2} \int dE E \left[\frac{1}{N_{\text{CB}}} \sum_i^{N_{\text{CB}}} g_{\text{CB}}^i(E) + \frac{1}{N_{\text{VB}}} \sum_j^{N_{\text{VB}}} g_{\text{VB}}^j(E) \right], \quad (4)$$

where the band-resolved DOS (normed to unity) is given as

$$g^i(E) = \frac{1}{N_{\mathbf{k}}} \sum_{\mathbf{k}} \delta[E - E^i(\mathbf{k})]. \quad (5)$$

In contrast to the Green's function method, Eq. (4) is also applicable to cases where the BP lies outside the band gap, as for example in InAs or InN. The pinning of the Fermi level near the branch point then results in electron accumulation at free surfaces, which can be observed by means of high-resolution electron-energy-loss spectroscopy (HREELS).^{36–38}

To sum it up, the calculation of BPs requires the choice of an appropriate input band structure [when using Eq. (2)] or DOS [Eq. (4)] and in practice the choice of a proper subset of contributing bands around the band gap region. For realistic band structures, the occurrence of Van Hove singularities due to the vanishing slope of non-(quasi-)crossing bands at the BZ boundaries will further complicate the problem, as dense \mathbf{k} -point samples are required to represent such kinks in the DOS. On the other hand, the typically shallow dispersion at the zone faces is of crucial influence to the branch point position,

as localized levels sample large \mathbf{k} -space regions. The usage of simple effective mass or $\mathbf{k} \cdot \mathbf{p}$ models is suitable for describing direct optical transitions near the Γ -point, but of little help here due to the erroneous dispersion for large wave vectors. Consequently, also the common use of nonlinearly-spaced Γ -centered meshes in more costly (e.g. quasiparticle) calculation schemes could in some cases counteract the accuracy of the BP calculation, as they typically give the largest \mathbf{k} -density in the least contributing BZ region. Furthermore, it is well known that even highly-sophisticated ab initio calculation schemes still struggle with the quantitative reproduction of electronic features of semiconductors.³⁹

As trade-off, empirical tight-binding models (ETBMs)⁴⁰ seem to be well-suited,³² as they allow for a realistic dispersion throughout the whole BZ, combined with a flexible parametrization scheme. Unfortunately, most ETBM parametrizations are also optimized to reproduce the zone center properties rather than those at the BZ boundaries.

To overcome these adversities, there exists a parametrization scheme by Loehr⁴¹ that fits the band structure of zincblende type crystals to the X -point energies within a small basis set of Wannier-like bonding orbitals on the Bravais lattice sites of the underlying crystal. For the wurtzite structure, a similar approach even allows for the fit of one CB and three VBs to almost all high-symmetry points in the hexagonal BZ, as the low crystal symmetry allows for a large number of independent parameters.⁴²

Although the ETBM by Loehr is well suited for the calculation of electronic and optical properties for a wide range of material systems and geometries,^{42–48} we found it to be of lower accuracy in the specific case of BP calculations for zb-CdSe and especially ZnTe. Due to the large spin-orbit coupling constant (the spin-orbit splitting of ZnTe at $\mathbf{k} = \mathbf{0}$ is about 1 eV),⁴⁹ the L -point energies do not coincide well with literature values⁴⁹ when not fitted explicitly. In this paper, we will therefore follow a modified approach within the same basis set. We fit one CB and three VBs, namely the heavy hole (HH), light hole (LH) and split-off band, of the zincblende band structure to the zone center masses and the energies at Γ and X , and additionally fix the position of the CB, HH and LH VB at L . More details are given in Appendix A.

C. Experimental determination of valence band offsets from type-II PL spectra

In order to obtain the VBO from photoluminescence measurements of the CdSe/ZnTe type-II interface, one has to take into account the special behavior of the charge carriers at the interface. Due to the type II band alignment, photo-generated electrons are confined in CdSe, while the holes are confined in ZnTe. Their attractive Coulomb force leads to an accumulation at the interface which causes an electric field E_{field} that is proportional to

the population of carriers n at the type-II interface, similar to a plate capacitor. This field can be described by a band-bending, which can be approximated for a planar type II interface as a triangular potential well.⁵⁰

The recombination rate Γ (a mix-up with the notation for the BZ center can be excluded in the context of this section) of charge carriers depends of course on the wave-function overlap between electrons and holes at the interface. At a type II interface, this overlap becomes a function of the charge carrier density at the interface. In Ref. 51, Shuvayef et al. present the charge carrier dynamics of a type II system obtained by a numerical solution of the self-consistent Schrödinger-Poisson system of equations. Their numerical results fit the experimental results very nicely. In this work, we propose a model that displays a comparably good agreement between theory and experiment, but by using an analytical solution of the carrier dynamics of a type II interface.

To obtain the dependency of the recombination rate Γ on the carrier population, we numerically solved the Schrödinger equations to get the overlap between electron and hole wavefunctions for different electric fields. The overlap has been found to be proportional to the electric field E_{field} at the interface,⁵² therefore the recombination rate Γ becomes proportional to the carrier density n . Then we can introduce a constant γ such that $\Gamma = \Gamma(n) = \gamma n$.

Next to be considered is the type of emission observed at a type II interface. The usual case for (in \mathbf{k} -space) direct or indirect band gap semiconductors at low temperatures and low excitation conditions is the observation of excitonic emission. With strongly increasing pumping power, the excitonic emission will evolve into a band-to-band emission (electron-hole plasma). For an emission from a type II interface this behavior is different, because the formation of excitons is hindered at low excitation conditions: Degani and Farias calculated in Ref. 53 the binding energy of an exciton at the type II interface of AlAs/GaAs under the assumption of infinite potential barriers for electrons and holes at the interface. They found the binding energy to increase with excitation power, but to be zero for excitation densities below a certain threshold. For finite barriers they estimate a general increase of the binding energy, leading to a lower threshold excitation density for the formation of excitons. Therefore, in our results, one has to expect a band-to-band transition (with a bimolecular recombination behavior) to be the main origin of the type II PL with an excitonic feature eventually coming up with increasing pumping power.

Starting from a rate equation for band-to-band recombination one can derive a description of the type II recombination dynamics by including the above mentioned carrier dependent recombination rate γn under the assumption of an equal electron and hole population ($n = p$):

$$\frac{dn}{dt} = \alpha P - (\gamma n)(n p) = \alpha P - \gamma n^3. \quad (6)$$

Here, P is the optical pumping power and α a proportionality factor. The solution to this equation is a hyperbolic function. Its time derivative itself gives the observable PL-intensity $I = dn/dt$ which very nicely describes the experimentally found non-exponential decay behavior. This is the first of two typical features for a type II emission,

$$I(t) = \frac{\gamma n_0^2}{(1 + \gamma n_0 t)^{3/2}}, \quad (7)$$

with $n_0 = n(t = 0)$. Solving the steady-state case of Eq. (6) for n gives the excitation power dependence of the number of generated charge carriers:

$$n = \left(\frac{\alpha P}{\gamma}\right)^{1/3}. \quad (8)$$

As described above, their attractive Coulomb interaction leads to an accumulation of charge carriers along the interface, creating a band bending which can be described as a triangular potential well.⁵⁰ In such a potential the charge carriers experience a confinement E_c which is a function of the electric field which itself is proportional to the number of charge carriers $E_c \propto E_{\text{field}}^{2/3} \propto n^{2/3}$. Accordingly, the dependence of the confinement energy on the optical pumping power is given by $E_c \propto P^{2/9}$. This confinement leads to a blueshift of the PL signal which is the second typical feature of a planar type II interface. The position of the PL signal $E(P)$ can then be fully described by

$$E(P) = E_0 + \beta P^{2/9}, \quad (9)$$

where E_0 is the zero-excitation, spatially indirect band gap of the type II junction and β a proportionality factor. The decay dynamics of the PL emission at a type II interface strongly resembles the behavior of an electron-hole plasma, but can be observed well below the Mott transition and show a much longer lifetime.

IV. RESULTS

A. ETBM band structure of zb-CdSe and ZnTe

Figure 1 shows the band structure and the DOS of zb-CdSe and ZnTe as obtained in our ETBM. Due to time inversion symmetry, all bands carry an additional twofold degeneracy throughout the whole BZ. More details on the parametrization and the input parameters can be found in the appendix of this work.

The fundamental influence of the spin-orbit coupling can easily be identified by the large energetic separation of the split-off band from the degenerate HH/LH at Γ . Also, the energetic regions with "flat" bands that contribute significantly to the DOS integrals and therefore also to the position of the BP can be located, e.g. around the X point for the VBs.

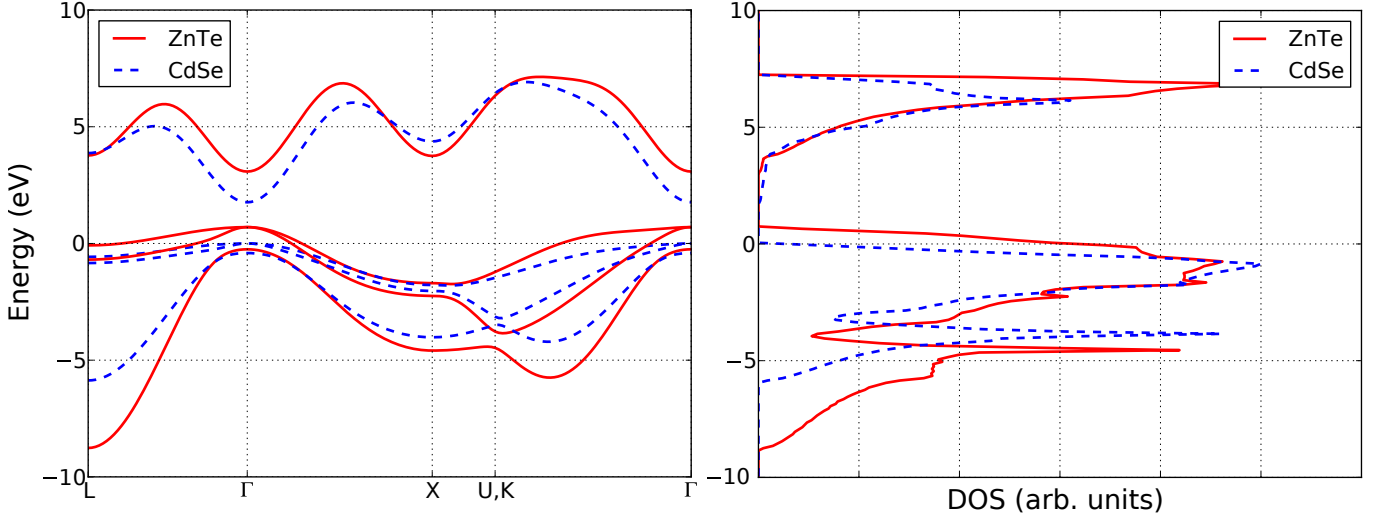


FIG. 1: (Color online) Band structures (left) and DOS (right) of zb-CdSe and ZnTe as obtained in our ETBM. Note that we already use the later calculated VBO of $E_v \approx 0.7$ eV in these plots.

As our ETBM as given in the appendix does not fix the split-off VB at L , it dips relatively far down there for ZnTe. Although it is also possible to fit the ETBM to this value, we are then left with a worse reproduction of the dispersion of this band at Γ (not shown here). Due to included band-mixing effects, this also implicitly influences the HH/LH VB dispersion and can lead to erroneous curvatures along Γ - X for ZnTe. We found the present parametrization to be most suitable for a good agreement of the DOS in comparison to literature data (see e.g. Ref. 49), as the overall shape is then very well reproduced besides a small "tail" of the lowest ZnTe VB on the low energy side. Its influence has been included in the error range for the calculated BPs and VBOs by comparing the respective results from either parametrizations.

In case of zb-CdSe, this problem does not occur. Here, the dispersion of the split-off band is well reproduced throughout the BZ including the zone boundaries without an additional fit to L when compared to available literature data.⁴⁹

B. Calculation of branch points and valence band offsets of zb-CdSe/ZnTe heterojunctions

As Schleife et al. pointed out in Ref. 14, the number of used bands can introduce a relevant uncertainty when calculating the BP energies. Figure 2 exemplary shows the band-resolved DOS of zb-CdSe. As the bandwidths of all bands are of comparable magnitude, we will use one CB and all three VBs per spin direction in our BP calculations. This also agrees well with the notion that in the zincblende structure the bands around the gap are mainly formed from one s orbital of the cation and three p orbitals of the anions on each unit cell.⁵⁴⁶⁵

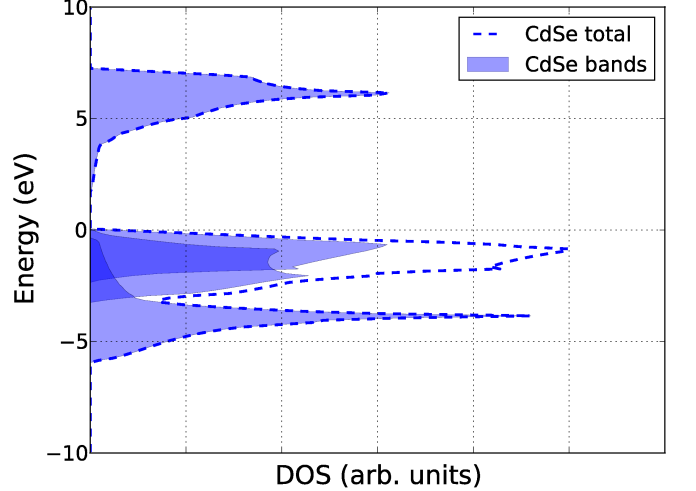


FIG. 2: (Color online). Band-resolved DOS of zb-CdSe.

The branch point calculation with the Green's function approach, Eq. (2), turns out not to be suitable for the material system under consideration, as satisfactory convergence of $G^{\mathbf{R}}(E)$ could not be achieved for either material, regardless of the interface orientation. When using the approximate formula (4), it turns out that the BP of zb-CdSe lies slightly above the CB edge, so that Eq. (2) is not applicable. In case of ZnTe, it is most likely a numerical problem, as the multiple kinks in the DOS of the VBs render $G^{\mathbf{R}}(E)$ extremely sensitive to the \mathbf{k} -resolution. Similar problems are reported in the literature.¹⁴ In contrast, convergence for the branch point energy E_{BP} is easily reached with Eq. (4).

The results can be found in Table I, together with literature data from a comprehensive work from Mönch.³² As

TABLE I: Resulting branch point energies E_{BP} from our specific ETBM with the BZ average approach. The literature values were taken from Ref. 32. All values are in eV. The two decimals are given for the sake of comparison and do not reflect the overall accuracy of the calculations (see text for details).

Material	E_{BP} (This work)	E_{BP} (Literature)
zb-CdSe	1.83	1.53
zb-ZnTe	1.09	0.73, 0.84, 1.00

mentioned above, our BP energy $E_{BP} = 1.83$ eV for zb-CdSe lies above the low-temperature CB edge at 1.76 eV, while the available literature value lies slightly below the CB minimum.

Nevertheless, taking into account the multiple sources of ambiguities in the BP calculations [e.g. uncertainties in the input parameters, the band structure parametrization and the loss of the slight, but present directional dependence of E_{BP} in Eq. (4)], we estimate the accuracy of the values to ± 0.1 eV, so that we cannot decisively conclude whether the BP really lies in the CB until suitable experimental evidence will be given, e.g. on electron accumulation on CdSe surfaces.

The result from Mönch also refers the cubic modification, but it has been calculated with a different tight-binding parametrization based on multiple previous works.^{55–57} Specifically, the there employed tight-binding matrix elements need to be rescaled with a heuristic factor in order to satisfactorily reproduce the electronic structure of chalcogenides. In addition, it is also not obvious how a change in temperature affects these values, as the band structure will in general be temperature-dependent. On the other hand, the lack of reliable material data for metastable materials and their temperature dependence adds another source of uncertainty also on our side.

Similarly, the available literature values for ZnTe are all smaller than our value $E_{BP} = 1.09$ eV. The first and the second value, however, originally stem from LMTO and LAPW calculations, respectively, and will therefore most likely suffer from the well-known issues with quantitative predictions in these models.

Altogether, the charge neutrality condition leaves us with an estimated VBO of

$$\Delta E_v \approx E_{BP}^{CdSe} - E_{BP}^{ZnTe} = (0.7 \pm 0.2) \text{ eV}. \quad (10)$$

The quantitative influence of corrections due to non-vanishing interface dipoles²⁹ can be estimated from the electronegativity values from Miedema et al.⁵⁸ and turns out to be small enough to be neglected (see Appendix B for details). Further corrections could be expected from the absence of a common atom across the interface, as the inevitable presence of Cd–Te and Zn–Se bonds in one layer could in principle introduce an additional confinement potential.^{59,60} This effect would also introduce an additional directional dependence, as has been reported

in Ref. 61.

Nevertheless, the detailed theoretical studies of Lambrecht and Segall³¹ at the example of polar InAs/GaSb interfaces come to the conclusion that for isovalent interfaces without common anion no mentionable electric field will result from these additional bonding configurations. This is also in accordance with the studies of Priester et al., who explicitly quantified the effect of an additional interface layer on the band offset of the $Al_xIn_{1-x}As/InP$ heterojunction by means of self-consistent tight-binding calculations.⁵⁹

As a generalization, Lambrecht and Segall find that details of the interface bonding configuration are only relevant for nonisovalent heterojunctions (like II-VI/IV). Then the polarity of the interface can play an important role and additional dipole corrections can be relevant. However, these consideration were made for cubic materials. In systems with lower crystal symmetry, the direction-dependent bonding geometry and stoichiometry of different surfaces might also play a role in case of isovalent heterojunctions.

C. Experimentally determined valence band offset

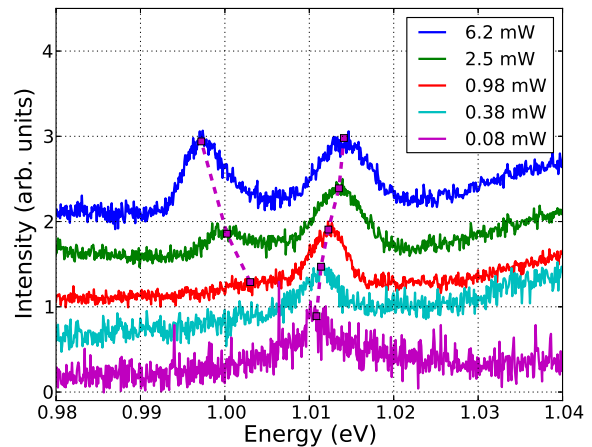


FIG. 3: (Color online). PL spectra of the type II interface obtained under various excitation powers at 6 K. The higher energy peak can be attributed to the type II interface recombination (showing a blueshift with increasing excitation power). The lower energy peak is probably the free exciton at the type II interface (showing a net redshift due to the influence of the exciton binding energy).

Figure 3 displays the PL signal from the type II interface between CdSe and ZnTe. This spatially indirect transition is 3–4 orders of magnitude weaker in comparison to the direct transitions in CdSe and ZnTe. The spectrum consists of two peaks, one which is visible at all excitation densities, and one which only becomes visi-

ble for large excitation densities and is positioned on the lower energy side of the first peak.

The higher energy peak is the type II band-to-band transition, which can be identified by its excitation dependence. The PL of a planar type II interface shows a blueshift [as described in Eq. (9)] and a hyperbolic decay behavior. The blueshift is clearly visible in Fig. 3, but the PL signal of the samples presented in this work was too weak to be investigated with time-resolved methods. However, we were able to create superlattices of CdSe/ZnTe in which the type II transition is shifted into the visible region of the spectrum. Such samples show a blueshift of the PL signal and a hyperbolic decay of the PL signal according to Eqns. (9) and (7), respectively, as is displayed in Fig. 4.

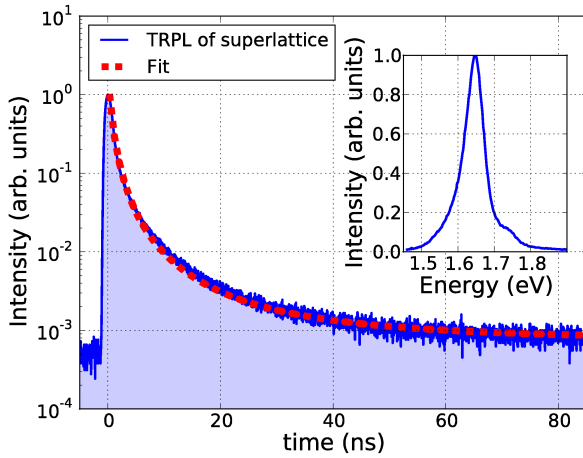


FIG. 4: (Color online). Decay behavior of the type II PL signal from a superlattice fabricated of 80 periods of 15 monolayers CdSe / 7 monolayers ZnTe. The dotted red curve is a fit according to Eq. (7). The signal has a very slow decay compared to the direct transitions in CdSe and ZnTe, respectively ($\tau < 2$ ns, not shown). The inset displays the time-integrated spectrum of this superlattice. The strongest peak at 1.65 eV is the PL of the type II transition.

The lower energy peak is only visible above a certain excitation density threshold. There are several hints that this line is the PL of the free exciton at the type II interface: The decay dynamics of the free exciton are slightly different from the band-to-band transition and result in a squared-hyperbolic (bimolecular-like) decay and a shift of the PL position $E(P) = E_0 + \beta P^{1/3} + E_{\text{bind}}(P)$ which includes the binding energy of the exciton at the type II interface E_{bind} . The binding energy is itself dependent on the pumping power and can be described by a power-law $E_{\text{bind}} \propto P^{0.12}$ (extracted from Fig. 2 in Ref. 53). This results in a net redshift of this line with increasing excitation density.

When comparing the calculated binding energy with the energy splitting between the two peaks found in our measurements, we can report a similar power-law be-

havior $E_{\text{bind}}(\text{CdSe/ZnTe}) \propto P^{0.08 \pm 0.1}$ with a maximum binding energy of $E_{\text{bind}} = 17$ meV at the highest excitation power. Of course, there are very few data points in our measurements, leaving room for improvements. Further indication for the exciton being the origin of this line lies in the excitation density dependent line intensity. The intensity of the band-to-band transition line (showing a blueshift) increases sub-linearly with the excitation density ($\propto P^{0.7 \pm 0.1}$), while the exciton line increases linearly with the excitation power ($\propto P^{1.0 \pm 0.1}$). This is typical for an excitonic emission. The sub-linear increase of the band-to-band transition could be explained by a strong nonradiative component for this transition, for example interface defects or Auger recombination. The summed intensity of both lines is still sub-linear. The last and strongest hint towards the exciton being the origin of the lower energy line is its eventual appearance above a certain threshold as it was predicted by Degani and Farias.⁵³

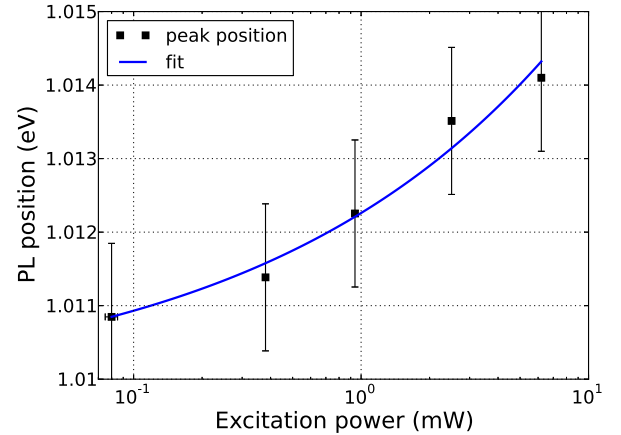


FIG. 5: (Color online). Shift of the type II band-to-band emission with increasing excitation power. The measurement data is shown as black squares. The curve is a power-law fit $E = E_0 + P^{2/9}$ according to Eq. (9). The determined zero-excitation band-gap is $E_0 = (1.01 \pm 0.01)$ eV.

Figure 5 shows the extracted blueshift of the band-to-band emission with the excitation power. The curve in Fig. 5 is a fit according to Eq. (9). The zero-excitation type II band-gap E_0 therefore is found to be

$$E_0 = (1.01 \pm 0.01) \text{ eV} . \quad (11)$$

Now the VBO for CdSe/ZnTe can simply be calculated as

$$\Delta E_v = E_g(\text{CdSe}) - E_0. \quad (12)$$

With the band-gap of cubic CdSe taken as $E_g(\text{CdSe}) = 1.76$ eV⁴⁹ the VBO for CdSe/ZnTe results to

$$\Delta E_v = (0.75 \pm 0.01) \text{ eV}. \quad (13)$$

D. Further Comparison Theory-Experiment-Literature

Our experimentally determined value of $\Delta E_v = (0.75 \pm 0.01)$ eV is larger than the one found in the measurement performed by Yu et al.,²¹ where a VBO of $\Delta E_v = (0.64 \pm 0.07)$ eV is reported (at room temperature, determined using XPS measurements) and also larger than the value by Gleim et al. from valence- and core-level photoelectron spectroscopy of (0.6 ± 0.1) eV.²² The difference between those results and our value for the VBO could be a result of the different temperatures at which the measurements were performed and in the case of Yu et al. also the small thickness of the CdSe layer used. Our calculated value for the VBO $\Delta E_v = (0.7 \pm 0.2)$ eV is in good agreement with the experimental findings presented in this work given the theoretical uncertainties of the method.

The determination of the VBO by measuring the type II PL emission is a very easy and precise method. Ostinelli et al. calculated in their work the VBO between InP and AlGaAsSb-alloys of various compositions using the type II transition²⁴ and come to a similar degree of precision for the VBO of these materials. Since the measurement of the PL with very high resolution is comparably easy, the main sources of error for the VBO determination lie in the evaluation of the PL shift. Here, mainly the range of excitation power which can be utilized with a given setup and the model used for the fitting determine the overall precision of the VBO calculation. Therefore, a good model of the type II emission is very important, not only to improve the precision of VBO calculations but to improve the understanding of the carrier dynamics at the type II interface in general. Of course, the accuracy of the literature values for the band gap of the constituents is also important, as they enter the analysis, see Eq. (12).

From the theoretical side, it should be noted that our usage of four sp^3 bonding-orbitals per Bravais lattice site of the zincblende structure represents a somewhat natural choice for the calculation of BPs. A detailed microscopic analysis of the bond structure across the surface as e.g. given in Ref. 31 shows that the BP can be identified with the average sp^3 hybrid level of the material. The dielectric screening of the charge transfer across the interface corresponds to a screening of the difference between these levels, which corresponds to an alignment of the branch points. Harrison and Tersoff pointed out that the more the lattice constants of the tetrahedral semiconductors are alike, the more accurate is this estimation of the band alignment.¹¹ The lattice constants of the cubic ZnTe/CdSe system under consideration differ by less than 0.2%, which may explain why this conceptionally rather simple theoretical approach gives especially good results in this case.

V. CONCLUSION AND OUTLOOK

In this paper, we have determined the valence band offset (VBO) of the CdSe/ZnTe type II heterojunction with underlying zincblende structure. As literature values for the VBO often show a huge spread, we have used a theoretical as well as an experimental approach to crosscheck our results.

On the experimental side, a model of the interface carrier dynamics has been used to extract an accurate value for the VBO from the excitation-power dependent photoluminescence (PL) signal of the type II interface. We have then obtained the value $\Delta E_v = (0.75 \pm 0.01)$ eV for the CdSe/ZnTe VBO, where the accuracy is essentially limited by the number of data points available from the experiment and the literature value of the bulk band gap for cubic bulk CdSe.

On the theoretical side, we have used a refined empirical tight-binding parametrization for the calculation of the branch point energy of cubic CdSe and ZnTe. The VBO has been determined to $\Delta E_v = (0.7 \pm 0.2)$ eV from the local charge neutrality condition. Here, the accuracy is predominantly limited by the included one-particle properties of the constituent materials, but the value confirms the experimental findings within its error boundaries.

As theoretical considerations from the literature suggest only a weak dependence on the interface polarity and orientation, we can in summary recommend the experimentally determined value of $\Delta E_v = (0.75 \pm 0.01)$ eV as zero-temperature VBO for the cubic CdSe/ZnTe heterojunction.

Our combined experimental and theoretical approach can in principle be applied to other type II heterojunctions. In case of systems with a lower crystal symmetry (e.g. wurtzite structure) and/or significantly larger lattice mismatch, possible dipole corrections and orientational dependencies may have to be considered on the theoretical side. On the experimental side, such conditions could lead to a stronger confinement of the charge carriers at the type II interface, in favor of the formation of excitons. In that case, the model of the carrier dynamics has to be corrected accordingly. In all cases, a careful analysis of the charge carrier dynamics at the interface is crucial to determine the VBO from power dependent PL measurements.

Acknowledgments

Daniel Mourad would like to thank Gerd Czycholl and Paul Gartner for fruitful discussions. Jan-Peter Richters would like to acknowledge financial support from CEA/DSM-energie.

Appendix A: Tight-binding parametrization

Our ETBM parametrization for the zincblende structure uses the same basis set as Loehr,⁴¹ i.e. a localized Wannier-type sp^3 basis per spin direction:

$$|\mathbf{R}\alpha\rangle, \quad \alpha \in \{s, p_x, p_y, p_z\} \times \{\uparrow, \downarrow\}. \quad (\text{A1})$$

Here, \mathbf{R} labels the sites of the fcc lattice, which is the underlying Bravais lattice of the zincblende structure. We basically follow the approach as described in Ref. 41, but with some modifications:

1. We do not use the two-center approximation.
2. In addition to the inclusion of second-nearest neighbors, we also include non-vanishing CB hopping matrix elements to $\mathbf{R} = a/2(2, 2, 0)$ and equivalent points, where a is the conventional lattice constant. This enables us to fit the CB to the L -point. The inclusion of the actual third-nearest neighbors at $\mathbf{R} = a/2(2, 1, 1)$ and equivalent points would in principle also be possible. However, we prefer the first choice: It prevents an erroneous CB dispersion along K - Γ that we do not wish to fix by a fit to the U, K point, as the corresponding energies are rarely known for most material systems.
3. The CB and the VBs are decoupled by setting all hopping matrix elements (ME) between s and p orbitals to zero.
4. The HH/LH VBs are not fitted to the Luttinger parameter γ_3 , i.e. we do not fit to the corresponding zone center effective masses along the $[111]$ direction.⁶⁶

Using the usual notation by Slater and Koster⁴⁰ for the matrix elements, we obtain:

$$\begin{aligned} E_{ss}^{000} &= \frac{3}{8} \Gamma_1^c + \frac{1}{4} L_1^c + \frac{3}{8} X_1^c + \frac{3}{2} \frac{\hbar^2}{a^2 m_c}, \\ E_{ss}^{110} &= \frac{1}{16} \Gamma_1^c - \frac{1}{16} X_1^c, \\ E_{ss}^{200} &= \frac{1}{48} \Gamma_1^c - \frac{1}{12} L_1^c + \frac{1}{16} X_1^c, \\ E_{ss}^{220} &= -\frac{1}{48} \Gamma_1^c + \frac{1}{48} L_1^c - \frac{1}{8} \frac{\hbar^2}{a^2 m_c}, \\ E_{xx}^{000} &= \frac{5}{8} \Gamma_{15}^v + \frac{1}{8} X_3^v + \frac{1}{4} X_5^v - 3 \frac{\hbar^2}{a^2 m_0} \gamma_1 + 4 \frac{\hbar^2}{a^2 m_0} \gamma_2, \\ E_{xx}^{110} &= \frac{1}{16} \Gamma_{15}^v - \frac{1}{16} X_3^v, \\ E_{xx}^{011} &= \frac{1}{16} \Gamma_{15}^v + \frac{1}{16} X_3^v - \frac{1}{8} X_5^v, \\ E_{xx}^{200} &= -\frac{1}{16} \Gamma_{15}^v + \frac{1}{16} X_3^v + \frac{1}{2} \frac{\hbar^2}{a^2 m_0} \gamma_1, \\ E_{xx}^{002} &= -\frac{1}{16} \Gamma_{15}^v + \frac{1}{16} X_5^v + \frac{1}{2} \frac{\hbar^2}{a^2 m_0} \gamma_1 - 2 \frac{\hbar^2}{a^2 m_0} \gamma_2, \\ E_{xy}^{110} &= -\frac{1}{4} \Gamma_{15}^v + \frac{1}{4} L_3^v + \frac{3}{2} \frac{\hbar^2}{a^2 m_0} \gamma_1 - 2 \frac{\hbar^2}{a^2 m_0} \gamma_2. \end{aligned} \quad (\text{A2})$$

TABLE II: Input material parameters for zb-CdSe and ZnTe. The double group notation is added in brackets if the corresponding energy values are identical.

Parameter	Description	CdSe	ZnTe
a	lattice constant (\AA)	6.077	6.089
Δ_{SO}	spin-orbit splitting (eV)	0.41	0.95
γ_1	Luttinger parameter	3.33	3.96
γ_2	Luttinger parameter	1.11	0.86
m_c	CB effective mass (m_0)	0.119	0.11
$\Gamma_1^c (\Gamma_6^c)$	CB energy (eV)	1.76	2.38
Γ_{15}^v	HH/LH VB energy (eV)	0	0
$X_1^c (X_6^c)$	CB energy (eV)	4.37	3.05
X_5^v	HH/LH VB energy (eV)	-1.78	-2.4
X_3^v	split-off VB energy (eV)	-4.0	-5.2
$L_1^c (L_6^c)$	CB energy (eV)	3.87	3.07
L_3^v	HH/LH VB energy (eV)	-0.71	-1.1

Here, m_0 is the free electron mass. The meaning of the remaining input parameters and the used values can be found in Table II. All values are taken from Ref. 49. The only exceptions are the Luttinger parameters for zb-CdSe, which are taken from Ref. 62, and the lattice constant of ZnTe to match the value as described in this paper for the present growth conditions.⁶⁷ We chose low-temperature input data where available (e.g. for the band gap) to ensure comparability with the experimental boundary conditions.

Note that the system of equations (A2) still uses the usual single group notation for the corresponding energy values. The addition of a spin-orbit coupling Hamiltonian H_{SO} on the same level of approximation as in Ref. 41 lifts degenerations. The topmost VB with single group symmetry Γ_{15}^v is split into a fourfold state Γ_8^v and a twofold state Γ_7^v , where

$$\Gamma_8^v - \Gamma_7^v = \Delta_{\text{SO}} \quad (\text{A3})$$

is the spin-orbit splitting constant. Similarly, the spin-orbit coupling splits the X_5^v edge to

$$X_7^v = X_5^v + \Delta_{\text{SO}}/3 \quad (\text{A4})$$

for the HH band. These analytically calculable linear shifts are being included explicitly into the set of equations (A2) by substitution. While the conduction band energies $\Gamma_1^c (= \Gamma_6^c)$, $X_1^c (= X_6^c)$ and $L_1^c (= L_6^c)$ remain unaffected by the spin, the shifts $X_5^v \rightarrow X_6^v$ (LH), $L_3^v \rightarrow L_{4,5}^v$ (HH) and $L_3^v \rightarrow L_6^v$ (LH) stem from higher-order roots of the characteristic polynomial and are only included implicitly via H_{SO} .

As usual, the band structure $E_n(\mathbf{k})$ is then obtained by diagonalization of the tight-binding matrix $\sum_{\mathbf{R}} \exp(i\mathbf{k} \cdot \mathbf{R}) E_{\alpha\alpha'}^{lmn}$ for each \mathbf{k} in the irreducible BZ.

Appendix B: Estimation of the interface dipole contribution

To estimate the contribution from interface dipoles, we closely follow Refs. 29,32. There, the VBO including dipole corrections is given as

$$\Delta E_v = E_{BP}^B - E_{BP}^A + D_x(X_B - X_A). \quad (B1)$$

Here X_A and X_B are electronegativity values from the Miedema scale and

$$D_x = \frac{A_x}{1 + 0.1(\varepsilon_\infty - 1)^2}, \quad (B2)$$

where $A_x = 0.86$ eV/Miedema-unit is the proportionality factor between the work function and the electronegativity, while ε_∞ is the optical dielectric constant of the semiconductor. The $X_{A/B}$ for binary compound semiconductors are obtained as the geometric mean of their constituents' values.

Using the data from Table A.4 of Ref. 63, we obtain $X_{CdSe} = (4.05 \times 5.79)^{1/2} \approx 4.84$ and $X_{ZnTe} =$

$(4.10 \times 4.92)^{1/2} \approx 4.49$. Here, the Miedema electronegativity values for Se and Te have been obtained from the corresponding Pauling values by the approximate conversion $X_{Mied} \approx 1.93 X_{Paul} + 0.87$, see e.g. Eq. (5.19) of Ref. 29. The low-temperature dielectric constants for zb-CdSe and ZnTe are approximately 7.8 and 6.7.⁶⁸ We use the first value, as the ZnTe valence electrons exponentially decay into the CdSe barrier. Then, the correction term $D_x(X_{CdSe} - X_{ZnTe})$ is approximately +0.05 eV. This value just falls in the accuracy range of the charge neutrality condition as mentioned in Sec. III A.

Although the calculated and the measured VBO for the CdSe/ZnTe junction would coincide almost perfectly when this dipole term is taken into account, we refrain from doing so (as common in the literature for junctions between isovalent semiconductors)²⁹. First, additional empirical parameters and assumptions enter the calculation of this contribution. Second, it would pretend a false degree of accuracy, as the calculation of the branch point itself is subject to several sources of uncertainties, as mentioned throughout this paper.

* Electronic address: dmourad@itp.uni-bremen.de

- ¹ G. G. Zegrya and A. D. Andreev, Applied Physics Letters **67**, 2681 (1995), .
- ² I. L. Kuskovsky, W. MacDonald, A. O. Govorov, L. Mourokh, X. Wei, M. C. Tamargo, M. Tadic, and F. M. Peeters, Physical Review B **76**, 035342 (2007) .
- ³ I. R. Sellers, V. R. Whiteside, I. L. Kuskovsky, A. O. Govorov, and B. D. McCombe, Physical Review Letters **100**, 136405 (2008) .
- ⁴ Y. Zhang, Wang, and A. Mascarenhas, Nano Letters **7**, 1264 (2007).
- ⁵ J. Schrier, D. O. Demchenko, Wang, and A. P. Alivisatos, Nano Letters **7**, 2377 (2007).
- ⁶ S.-H. Wei and A. Zunger, Applied Physics Letters **72**, 2011 (1998).
- ⁷ R. Anderson, Solid-State Electronics **5**, 341 (1962).
- ⁸ J. A. Van Vechten, Physical Review **187**, 1007 (1969).
- ⁹ C. G. Van de Walle and R. M. Martin, Physical Review B **34**, 5621 (1986).
- ¹⁰ C. G. Van de Walle, Physical Review B **39**, 1871 (1989).
- ¹¹ W. A. Harrison and J. Tersoff, Journal of Vacuum Science & Technology B: Microelectronics and Nanometer Structures **4**, 1068 (1986).
- ¹² M. Cardona and N. E. Christensen, Physical Review B **35**, 6182 (1987).
- ¹³ C. G. Van de Walle and J. Neugebauer, Nature **423**, 626 (2003).
- ¹⁴ A. Schleife, F. Fuchs, C. Rödl, J. Furthmüller, and F. Bechstedt, Applied Physics Letters **94**, 012104 (2009).
- ¹⁵ B. Höfiling, A. Schleife, F. Fuchs, C. Rödl, and F. Bechstedt, Applied Physics Letters **97**, 032116 (2010).
- ¹⁶ W. Mönch, Journal of Applied Physics **109**, 113724 (2011).
- ¹⁷ S. Kim, B. Fischer, H. J. Eisler, and M. Bawendi, Journal of the American Chemical Society **125**, 11466 (2003).
- ¹⁸ C. K. Shih and W. E. Spicer, Physical Review Letters **58**,

- 2594 (1987).
- ¹⁹ D. Biswas, N. Debbar, P. Bhattacharya, M. Razeghi, M. Defour, and F. Omnes, Applied Physics Letters **56**, 833 (1990).
- ²⁰ D. V. Lang, M. B. Panish, F. Capasso, J. Allam, R. A. Hamm, A. M. Sergent, and W. T. Tsang, Applied Physics Letters **50**, 736 (1987).
- ²¹ E. T. Yu, M. C. Phillips, J. O. McCaldin, and T. C. McGill, Journal of Vacuum Science & Technology B: Microelectronics and Nanometer Structures **9**, 2233 (1991).
- ²² Th. Gleim, L. Weinhardt, Th. Schmidt, R. Fink, C. Heske, E. Umbach, P. Grabs, G. Schmidt, L. W. Molenkamp, B. Richter, A. Fleszar, and H.- P. Steinrück, Applied Physics Letters **81**, 3813 (2002).
- ²³ P. Dawson, B. A. Wilson, C. W. Tu, and R. C. Miller, Applied Physics Letters **48**, 541 (1986).
- ²⁴ O. Ostinelli, G. Almuneau, and W. Bachtold, Semiconductor Science and Technology **21**, 681 (2006).
- ²⁵ E. R. Glaser, R. Magno, B. V. Shanabrook, and J. G. Tischler, Physical Review B **74**, 235306 (2006).
- ²⁶ Y. Park, R. Andre, J. Kasprzak, L. S. Dang, and E. Bellet-Amalric, Applied Surface Science **253**, 6946 (2007).
- ²⁷ N. Samarth, H. Luo, J. Furdyna, S. Qadri, Y. Lee, R. Alonso, E. Suh, A. Ramdas, and N. Otsuka, Surface Science **228**, 226 (1990).
- ²⁸ F. Flores and C. Tejedor, Journal of Physics C: Solid State Physics **12**, 731 (1979).
- ²⁹ W. Mönch, *Electronic Properties of Semiconductor Interfaces* (Springer, Berlin/Heidelberg, 2004), 1st ed.
- ³⁰ J. Tersoff, Physical Review B **30**, 4874 (1984).
- ³¹ W. R. L. Lambrecht and B. Segall, Physical Review B **41**, 2832 (1990).
- ³² W. Mönch, Journal of Applied Physics **80**, 5076 (1996).
- ³³ R. E. Allen, Physical Review B **20**, 1454 (1979).
- ³⁴ J. Tersoff, Physical Review Letters **52**, 465 (1984).

- ³⁵ J. Tersoff, *Physical Review B* **32**, 6968 (1985).
- ³⁶ M. Noguchi, K. Hirakawa, and T. Ikoma, *Physical Review Letters* **66**, 2243 (1991).
- ³⁷ I. Mahboob, T. D. Veal, L. F. J. Piper, C. F. McConville, H. Lu, W. J. Schaff, J. Furthmüller, and F. Bechstedt, *Physical Review B* **69**, 201307 (2004).
- ³⁸ L. F. J. Piper, T. D. Veal, M. J. Lowe, and C. F. McConville, *Physical Review B* **73**, 195321 (2006).
- ³⁹ P. Rinke, A. Qteish, J. Neugebauer, C. Freysoldt, and M. Scheffler, *New Journal of Physics* **7**, 126 (2005).
- ⁴⁰ J. C. Slater and G. F. Koster, *Physical Review* **94**, 1498 (1954).
- ⁴¹ J. P. Loehr, *Physical Review B* **50**, 5429 (1994).
- ⁴² D. Mourad, S. Barthel, and G. Czycholl, *Physical Review B* **81**, 165316 (2010).
- ⁴³ D. Mourad, G. Czycholl, C. Kruse, S. Klemmt, R. Retzlaff, D. Hommel, M. Gartner, and M. Anastasescu, *Physical Review B* **82**, 165204 (2010).
- ⁴⁴ O. Marquardt, D. Mourad, S. Schulz, T. Hickel, G. Czycholl, and J. Neugebauer, *Physical Review B (Condensed Matter and Materials Physics)* **78**, 235302 (2008).
- ⁴⁵ S. Schulz, D. Mourad, and G. Czycholl, *Physical Review B* **80**, 165405 (2009).
- ⁴⁶ D. Mourad and G. Czycholl, *The European Physical Journal B* **78**, 497 (2010).
- ⁴⁷ D. Mourad and G. Czycholl, *The European Physical Journal B - Condensed Matter and Complex Systems* **85**, 1 (2012).
- ⁴⁸ S. Schulz, D. Mourad, S. Schumacher, and G. Czycholl, *physica status solidi (b)* (2011).
- ⁴⁹ S. Adachi, *Handbook on Physical Properties of Semiconductors, Volume 3: II-VI Compound Semiconductors* (Springer-Verlag, Berlin/Heidelberg, 2004).
- ⁵⁰ W. W. Lui and M. Fukuma, *Journal of Applied Physics* **60**, 1555 (1986).
- ⁵¹ V. A. Shuvayev, I. L. Kuskovsky, L. I. Deych, Y. Gu, Y. Gong, G. F. Neumark, M. C. Tamargo, and A. A. Lisyansky, *Physical Review B* **79**, 115307 (2009).
- ⁵² R. André, J. Bleuse, L. Gérard, J. Richters, R. Najjar, and H. Mariette, unpublished (2012).
- ⁵³ M. H. Degani and G. A. Farias, *Physical Review B* **42**, 11701 (1990).
- ⁵⁴ S. Schulz and G. Czycholl, *Physical Review B* **72**, 165317 (2005).
- ⁵⁵ C. F. Fischer, *Atomic Data and Nuclear Data Tables* **4**, 301 (1972).
- ⁵⁶ W. A. Harrison, *Physical Review B* **24**, 5835 (1981).
- ⁵⁷ P. Vogl, H. P. Hjalmarson, and J. D. Dow, *Journal of Physics and Chemistry of Solids* **44**, 365 (1983).
- ⁵⁸ A. Miedema, P. de Châtel, and F. de Boer, *Physica B+C* **100**, 1 (1980).
- ⁵⁹ C. Priester, Y. Foulon, and G. Allan, *Physical Review B* **49**, 2919 (1994).
- ⁶⁰ A. S. Gurevich, V. P. Kochereshko, J. Bleuse, H. Mariette, A. Waag, and R. Akimoto, *Nanotechnology* **22**, 365707 (2011).
- ⁶¹ W. S. Su, M. H. Ya, Y. S. Chiu, and Y. F. Chen, *Physical Review B* **66**, 113305 (2002).
- ⁶² Y. D. Kim, M. V. Klein, S. F. Ren, Y. C. Chang, H. Luo, N. Samarth, and J. K. Furdyna, *Physical Review B* **49**, 7262 (1994).
- ⁶³ W. Mönch, *Semiconductor Surfaces and Interfaces* (Springer, Berlin/Heidelberg, 2001), 3rd ed.
- ⁶⁴ V. P. Gupta and N. M. Ravindra, *physica status solidi (b)* **100**, 715 (1980).
- ⁶⁵ In similar III-V and III-nitride compound semiconductors with zincblende structure, the split-off band shows a much larger dispersion with large contributions far below the VB edge, so that it should likely be dismissed when using only one CB per spin direction (see Ref. 14).
- ⁶⁶ Points 3 and 4 could render this parametrization less suitable for the calculation of optical properties than Loehr's scheme. For our branch point calculations however, the CB-VB coupling and the fit to [111] zone center masses can be neglected.
- ⁶⁷ The corresponding set of Luttinger parameters from Ref. 49 were estimated from a plot of the band gap versus the γ_i for cubic semiconductors. It might be suitable for effective mass and $\mathbf{k} \cdot \mathbf{p}$ models but leads to erroneous band curvatures for large \mathbf{k} .
- ⁶⁸ Please note that the value of $\varepsilon_\infty = 6.2$ from Adachi's data collection, Ref. 49, is not suitable here, as it is a directionally averaged result from wurtzite phase data at room temperature. In particular, the dielectric response should become larger when the bulk band gap becomes smaller. A possible approach to find consistent values for II-VI semiconductors is the use of the empirical Moss model as done by Gupta and Ravindra in Ref. 64. This has also successfully been applied to further II-VI systems, see Ref. 46. Our value for CdSe is also in satisfactory agreement with recent values in the Landolt-Börnstein database.